01 May 1996

# Dispersion Comparison for DSI- and Tensor-Based Nonorthogonal FDTD

Hao Shi

James L. Drewniak
*Missouri University of Science and Technology*, drewniak@mst.edu



## Recommended Citation

H. Shi and J. L. Drewniak, "Dispersion Comparison for DSI- and Tensor-Based Nonorthogonal FDTD," *IEEE Microwave and Guided Wave Letters*, vol. 6, no. 5, pp. 193-195, Institute of Electrical and Electronics Engineers (IEEE), May 1996.
The definitive version is available at https://doi.org/10.1109/75.491502

# Dispersion Comparison for DSI- and Tensor-Based Nonorthogonal FDTD

Hao Shi and James L. Drewniak

*Abstract*—**An explicit formulation of the finite-difference time-domain–discrete surface integral (FDTD–DSI) technique has allowed a rigorous study of numerical dispersion for the method. The study shows that the DSI- and tensor-based FDTD methods do not have the same numerical dispersion relation. It also clarifies the recently reported discrepancies in the dispersion relation between the two approaches. This study also shows that the tensor-based FDTD algorithm exhibits better dispersion properties for a two-dimensional uniformly skewed mesh.**

## I. Introduction

FINITE-difference time-domain (FDTD) [1]–[3] is a powerful numerical technique for solving many electromagnetic problems. The conventional FDTD Yee algorithm employing a rectangular grid is less efficient in handling complicated geometries when accuracy is required. Nonorthogonal FDTD methods that have been developed include the discrete surface integral (DSI) [4] and tensor-based algorithms [5], [6]. The numerical dispersion relation (NDR) for the Yee algorithm is well understood; however, the behavior of the NDR for nonorthogonal FDTD methods is less so. Due to the complexity of algebra associated with the derivation of a NDR in an arbitrary grid, a three-dimensional (3-D) or two-dimensional (2-D) uniformly skewed grid is often employed. Ray has provided an analytical formula for a general nonorthogonal algorithm on a 2-D uniformly skewed mesh [7]. A general formula for the NDR of the tensor-based FDTD method has been given by Navarro *et al.*, for a 3-D uniformly skewed mesh [8]. When applied to a 2-D uniformly skewed mesh, the NDR for the tensor-based FDTD [8] differs slightly from that given by Ray [7]. Navarro *et al.*, suggested a mistake in the derivation of [7]. However, this study shows that both results are correct and that the two methods in fact do not have the same dispersion relation.

An explicit formalism of FDTD-DSI has been developed [9] that allows a rigorous derivation of the NDR for the DSI method. For a 2-D uniformly skewed mesh, the results are consistent with those given by Ray [7]. Comparison of the dispersion relations indicates that the DSI- and tensor-based nonorthogonal FDTD methods behave distinctly, and the NDR presented by Ray [7] is applicable to the DSI-based method, while the formula given by Navarro *et al.*, [8] is applicable to the tensor-based method. Further, the tensor-based FDTD method exhibits less numerical dispersion than the FDTD-DSI method in the special case of a 2-D uniformly skewed grid.

Manuscript received October 10, 1995.

The authors are with the Department of Electrical Engineering, Electromagnetic Compatibility Laboratory, University of Missouri-Rolla, Rolla, MO 65401-0249 USA.

Publisher Item Identifier S 1051-8207(96)03432-0.

## II. Dispersion for FDTD–DSI Method

A detailed description of the DSI method can be found in the literature [4], [10], and only a brief summary is given here. A structured grid with hexahedral cells shown in Fig. 1 is employed here for demonstration, although the DSI method is generally applicable to unstructured grids. A secondary grid is introduced by taking the center-of-mass points of all cells in the primary grid (the initial grid) as nodes. The dotted lines in Fig. 1 are the primary edges, and the solid or dashed lines are the secondary edges. The $\vec{E}$-field is sampled along the primary edges and the $\vec{H}$-field along secondary edges. The integral form of Ampere's law applied on a loop in the secondary grid yields $\frac{\partial \vec{E}}{\partial t} \cdot \hat{n}$, where $\hat{n}$ is the unit face normal vector of a secondary cell-face. The effective face normal and area can always be uniquely defined, even if the four nodal points are nonplanar [9]. In general, a secondary face normal vector will not be aligned with its corresponding primary edge, as is the case for a Cartesian grid, complicating the $\vec{E}$-field time-marching scheme. First, Ampere's law is applied in all face-loops in the secondary grid to give $\frac{\partial \vec{E}}{\partial t} \cdot \hat{n}$ in the (secondary grid) face normal direction. Then, corresponding to each $\vec{E}$-field sampling Point $P$ along a primary edge $\vec{L}_P$, the $\frac{\partial \vec{E}}{\partial t} \cdot \hat{n}$ values at Point $P$'s nine (including the face Point $P$ is directly associated with) neighboring secondary faces are used to yield a vector quantity $(\frac{\partial \vec{E}}{\partial t})|_P$ thru an elaborate reconstruction and weighted-averaging procedure [4]. Finally, finite differencing in time yields $(\frac{\partial \vec{E}}{\partial t})|_P \cdot \hat{L}_P = \frac{E_P^{n+1} - E_P^n}{\Delta t}$, and a time-marching equation for $E_P$ results. The net consequence of the DSI algorithm is that the time-marching equation of $E_P$ is related to Point $P$'s 20 neighboring magnetic field components.

An explicit FDTD–DSI algorithm for a structured grid has been developed [9]. At any location with index $[i, j, k]$, the $\vec{E}$-field is represented by three scalar components $\{E_1, E_2, E_3\}$. The time-marching equation for one $\vec{E}$-field component is

$$E_1^{n+1}(i,j,k) = E_1^n(i,j,k) + \frac{\Delta t}{\epsilon_1(i,j,k)} \sum_{q=1}^{20} \tau_{1,q}^e H_{1,q}^{n+1/2} \quad (1)$$

where $\epsilon_1$ is the average value of permittivity for cell $(i, j, k)$, and $\tau_{1,q}^e$ are geometric coefficients incorporating contributions from the 20 surrounding $\vec{H}$-field components. Similar time-marching equations for the $\vec{H}$-field components can be

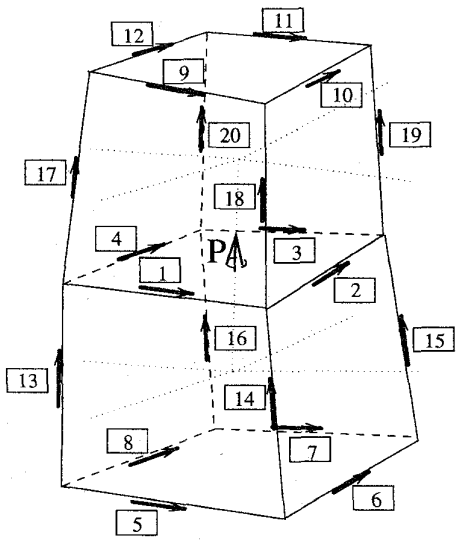


Fig. 1. A typical sampling point ($P$) of electric field $\vec{E}$ and its 20 neighboring magnetic-field components.

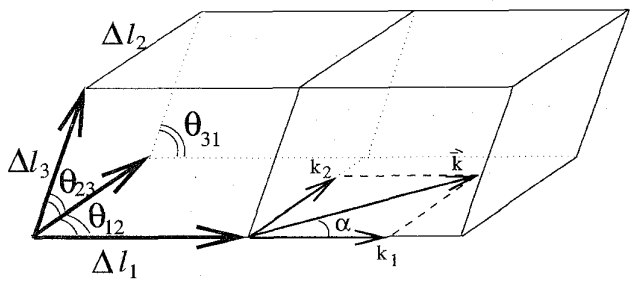


Fig. 2. Cell configuration for a 3-D uniformly skewed grid.

obtained with geometric coefficients $\tau_{1,q}^{h}$ incorporating contributions from the 20 surrounding $\vec{E}$-field components. The $\{\tau_{p,q}^{e}, \tau_{p,q}^{h}\}$ coefficients are determined by the mesh geometry, and explicit formulas are available [9]. For a 3-D uniformly skewed mesh defined by cell dimensions $\{\Delta l_1, \Delta l_2, \Delta l_3\}$ and angles between the basis vectors $\{\theta_{12}, \theta_{23}, \theta_{31}\}$ (as seen in Fig. 2) $\tau_{p,q}^{e} = \tau_{p,q}^{h} = \tau_{p,q}$ for $p = 1, 2, 3$, and $q = 1, 2, \ldots, 20$. The relations for $\tau_{p,q}$ are then relatively simple, for example $\tau_{1,1} = \frac{1}{V_{123}\Delta l_2 \Delta l_3}$, $\ldots$, $\tau_{1,5} = \frac{\cos\theta_{31}}{4V_{123}\Delta l_1 \Delta l_2}, \ldots$, $\tau_{1,13} = \frac{1}{4V_{123}\Delta l_1}(\frac{\cos\theta_{12}}{\Delta l_3} - \frac{\cos\theta_{31}}{\Delta l_2})$, $\ldots$, and $\tau_{1,17} = \frac{1}{4V_{123}\Delta l_1}(\frac{\cos\theta_{12}}{\Delta l_3} - \frac{\cos\theta_{31}}{\Delta l_2}), \ldots$ where $V_{123} = \hat{l}_1 \cdot (\hat{l}_2 \times \hat{l}_3) = (\Delta l_1 \cdot \Delta l_2 \cdot \Delta l_3)(1 - \cos^2\theta_{12} - \cos^2\theta_{23} - \cos^2\theta_{31} + 2\cos\theta_{12}\cos\theta_{23}\cos\theta_{31})^{1/2}$ is the unit cell volume.

Von Neumann's approach [11] is employed with the explicit FDTD-DSI formulation to analyze the dispersion properties of the algorithm. For a monochromatic plane wave with propagation vector $\vec{k}$ and frequency $\omega$ numerically propagating through the mesh, a time-harmonic solution for a field component is $E_1(i,j,k) = E_1^0(i,j,k)e^{J(\omega t - \vec{k}\cdot\vec{r})}$. Let $t = n\Delta t$, and, $\vec{r} = i\Delta l_1\hat{l}_1 + j\Delta l_2\hat{l}_2 + k\Delta l_3\hat{l}_3$, $\vec{k} = k_1\hat{l}_1 + k_2\hat{l}_2 + k_3\hat{l}_3$. Upon inserting the steady-state solution for all six field components into the time-marching equations of the explicit FDTD–DSI, a set of linear simultaneous equations in $\{E_1^0, E_2^0, E_3^0, H_1^0, H_2^0, H_3^0\}$ result [9]. Since $\{E_1^0, E_2^0, E_3^0, H_1^0, H_2^0, H_3^0\}$ are in general nonzero, the determinant must vanish, which yields the numerical dispersion relation. For the 2-D uniformly skewed grid analyzed by Ray, $\theta_{23} = \theta_{31} = 90°$, $k_3 = 0$, and the NDR is

$$\begin{aligned}\frac{1}{(c\Delta t)^2}\sin^2\left(\frac{\omega\Delta t}{2}\right) &= \frac{1}{\sin\theta_{12}{}^2} \times \left\{\frac{1}{(\Delta l_1)^2}\sin^2\left(\frac{k\Delta l_1\cos\alpha}{2}\right) + \frac{1}{(\Delta l_2)^2} \times \sin^2\left[\frac{k\Delta l_2\cos(\alpha-\theta_{12})}{2}\right] - \frac{1}{2}\frac{\cos\theta_{12}}{\Delta l_1\Delta l_2} \times \sin(k\Delta l_1\cos\alpha)\cdot\sin[k\Delta l_2\cos(\alpha-\theta_{12})]\right\}. \quad (2)\end{aligned}$$

where the relations $k_1 + k_2\cos\theta_{12} \rightarrow k\cos\alpha$, and $k_2 + k_1\cos\theta_{12} \rightarrow k\cos(\alpha - \theta_{12})$ are used, with $\alpha$ the angle of direction of wave propagation with respect to the $+\hat{x}_1$ axis, as seen in Fig. 2. Equation (2) is identical to that given by Ray [7].

## III. Comparison Between the Numerical Dispersion of FDTD-DSI and FDTD-Tensor Based Methods

The general NDR for the tensor-based nonorthogonal algorithm is

$$\frac{\sin^2\left(\frac{1}{2}\omega\Delta t\right)}{(c\Delta t)^2} = \sum_{i=1,j=1}^{3,3} g^{ij}\sin\left(\frac{k_i}{2}\right)\sin\left(\frac{k_j}{2}\right) \quad (3)$$

in terms of the conjugate metric tensor and the covariant components of $\vec{k}$ [6], [8]. In a 2-D uniformly skewed mesh, (3) can be simplified as

$$\begin{aligned}\frac{1}{(c\Delta t)^2}\sin^2\left(\frac{\omega\Delta t}{2}\right) &= \frac{1}{\sin\theta_{12}{}^2} \times \left\{\frac{1}{(\Delta l_1)^2}\sin^2\left(\frac{k\Delta l_1\cos\alpha}{2}\right) + \frac{1}{(\Delta l_2)^2}\sin^2\left[\frac{k\Delta l_2\cos(\alpha-\theta_{12})}{2}\right] - 2\frac{\cos\theta_{12}}{\Delta l_1\Delta l_2} \times \sin\left(\frac{1}{2}k\Delta l_1\cos\alpha\right) \cdot \sin\left[\frac{1}{2}k\Delta l_2\cos(\alpha-\theta_{12})\right]\right\}. \quad (4)\end{aligned}$$

The NDR's (2) and (4) for the two FDTD methods differ only in the last term on the right-hand sides. The last term of the NDR for the DSI-based FDTD method can be written as

$$\begin{aligned}&-2\frac{\cos\theta_{12}}{\sin^2\theta_{12}\Delta l_1\Delta l_2}\sin\left(\frac{1}{2}k\Delta l_1\cos\alpha\right) \times \sin\left[\frac{1}{2}k\Delta l_2\cos(\alpha-\theta_{12})\right] \\ &\times\cos\left(\frac{1}{2}k\Delta l_1\cos\alpha\right)\cos\left[\frac{1}{2}k\Delta l_2\cos(\alpha-\theta_{12})\right] \quad (5)\end{aligned}$$

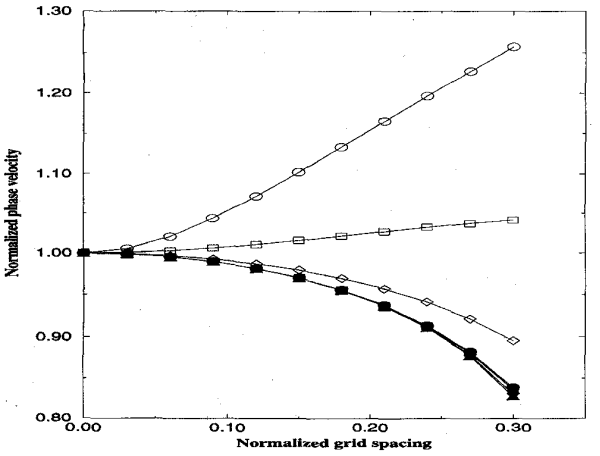


Fig. 3. Normalized phase velocity vs. the normalized grid spacing for $\alpha = 0$, $\theta = 45°(\bigcirc)$, $60°(\square)$, $75°(\diamond)$, and $90°(\triangle)$. The filled $\triangle$'s are exactly on top of the open $\triangle$'s. $c\Delta t/\Delta l = 0.5$.

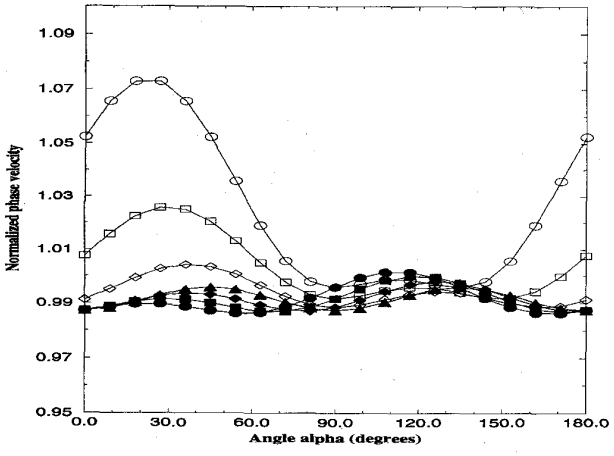


Fig. 4. Normalized phase velocity versus $\alpha$. $\theta = 45°(\bigcirc)$, $60°(\square)$, $75°(\diamond)$, and $90°(\triangle)$. The filled $\triangle$'s are exactly on top of the open $\triangle$'s. $c\Delta t/\Delta l = 0.5$, and $\Delta l/\lambda_0 = 0.1$.

and the real difference with that for the tensor-based FDTD method is a multiplier

$$\Lambda = \cos\left(\frac{1}{2}k\Delta l_1 \cos\alpha\right)\cos\left[\frac{1}{2}k\Delta l_2 \cos(\alpha - \theta_{12})\right]. \quad (6)$$

When $\alpha = 90°$ or $\alpha = \theta_{12} \pm 90°$, i.e., for waves propagating normal to one of the grid axes, the last term in the NDR for both methods vanishes, and the tensor-based FDTD and FDTD-DSI methods have the same NDR. The normalized phase velocity $v_p/c$ is plotted versus the normalized grid spacing $\Delta l/\lambda_0$ by Ray and Navarro *et al.* for varying mesh skewness. When $\Delta l/\lambda_0 \to 0$, $v_p/c \to 1$ and the continuous dispersion relation is recovered.

In most cases $\Lambda \neq 0$, and the tensor-based FDTD and FDTD–DSI have different NDR's. The normalized phase velocity is plotted versus the normalized grid spacing in Fig. 3 with an angle of propagation $\alpha = 0$ for several values of $\theta$. In Figs. 3 and 4, the filled and open symbols are for the tensor-based and DSI-based FDTD methods, respectively. Fig. 3 illustrates that the DSI- and tensor-based methods have significantly different dispersion characteristics. The DSI-based method is sensitive to a change of $\theta$. For $\theta = 45°$ and $\alpha = 0°$, the normalized phase velocity for $\Delta l/\lambda_0 = 0.1$ deviates as much as 5% from unity. Conversely, the tensor-based method is less sensitive to a change in $\theta$, with a deviation of the normalized phase velocity from unity of about 1% for $\Delta l/\lambda_0 = 0.1$. The normalized phase velocity is plotted versus $\alpha$ in Fig. 4 for several values of $\theta$ and $\Delta l/\lambda = 0.1$. The maximum deviation of the normalized phase velocity from unity is about 7% for the DSI-based method and 0.5% for the tensor-based method. Overall, these results indicate that the FDTD tensor-based method exhibits less dispersion than the FDTD DSI-based method for a 2-D uniformly skewed grid.

## IV. Conclusion

This study has demonstrated that the tensor- and DSI-based nonorthogonal FDTD methods do not have the same NDR. The NDR presented by Ray [7] is correct for DSI-based FDTD method, while the NDR presented by Navarro *et al.* [8] is correct for the tensor-based FDTD method. The tensor-based FDTD method exhibits less numerical dispersion than that of the DSI-based method for the 2-D uniformly skewed mesh studied, and similar results might be expected in 3-D. The DSI method, however, is very general and applicable to an unstructured mesh. Improvements in the NDR of the DSI method might be obtained by modifying the vector reconstruction and averaging scheme of the algorithm.

## References

[1] A. Taflove, *Computational Electrodynamics—The Finite-Difference Time-Domain Method.* Boston, MA: Artech House, 1995.
[2] K. S. Kunz and R. J. Luebbers, *The Finite Difference Time Domain Method for Electromagnetics.* Boca Raton, FL: CRC, 1993.
[3] K. L. Shlager and J. B. Schnelder, "A selective survey of the finite-difference time-domain literature," *IEEE Antennas Propagat. Mag.*, vol. 37, no. 4, 1995.
[4] N. K. Madsen, "Divergence preserving discrete surface integral methods for Maxwell's curl equations using nonorthogonal unstructured grids," *J. Computational Phys.*, vol. 119, pp. 34–45, 1995.
[5] R. Holland, "Finite-difference solution of Maxwell's eqution in generalized nonorthogonal coordinates," *IEEE Trans. Nucl. Sci.*, vol. 30, pp. 4589–4591, 1983.
[6] J.-F. Lee, R. Palandech, and R. Mittra, "Modeling three-dimensional discontinuities in waveguides using nonorthogonal FDTD algorithm," *IEEE Trans. Microwave Theory Tech.*, vol. 40, pp. 346–352, 1992.
[7] S. L. Ray, "Numerical dispersion and stability characteristics of time-domain methods on nonorthogonal meshes," *IEEE Trans. Antennas Propagat.*, vol. 41, pp. 233–235, 1993.
[8] E. A. Navarro, C. Wu, P. Y. Chung, and J. Litva, "Some considerations about the finite difference time domain method in general curvalinear coordinates," *IEEE Microwave Guided Wave Lett.*, vol. 4, pp. 396–398, 1994.
[9] H. Shi, "Study of printed circuit and waveguide coupler discontinuities with an FDTD-discrete surface integral method," M.S. thesis, University of Missouri-Rolla, 1995.
[10] S. D. Gedney and F. Lansing, in A. Taflove, *Computational Electrodynamics—The Finite-Difference Time-Domain Method.* Boston, MA: Artech House, 1995, pp. 369–392.
[11] W. T. Vetterling W. H. Press, S. A. Teukolsky, and P. Flannery, *Numerical Recipes in C.* Cambridge: Cambridge Univ. Press, 1990.